

引用格式: ZHAO Xiaopeng, HUANG Chongjia, HAO Peng. Tunable High-order Subharmonic Injection-locked Optoelectronic Oscillator in K-band Based on a Dual-polarization Mach-Zehnder Modulator[J]. Acta Photonica Sinica, 2026, 55(3):0355111

赵晓鹏, 黄崇佳, 郝鹏. 基于双偏振马赫-曾德尔调制器的 K 波段可调谐高阶亚谐波注入锁定光电振荡器[J]. 光子学报, 2026, 55(3):0355111

# 基于双偏振马赫-曾德尔调制器的 K 波段可调谐 高阶亚谐波注入锁定光电振荡器

赵晓鹏<sup>1,2</sup>, 黄崇佳<sup>1,2</sup>, 郝鹏<sup>1,2</sup>

(1 河北大学 物理科学与技术学院, 光信息技术创新中心, 保定 071002)

(2 河北省光学感知技术创新中心, 保定 071002)

**摘要:** 提出并实验验证了一种基于双偏振马赫-曾德尔调制器的亚谐波注入锁定光电振荡器系统。高阶亚谐波射频信号通过双偏振马赫-曾德尔调制器对光载波的 X 偏振态进行调制, 调制后的光信号在光电探测器进行光电转换、经过带通滤波器滤出某一高阶谐波信号, 产生与光电振荡器同频的射频信号。该射频信号注入基于光载波 Y 偏振态构建的光电振荡环路中, 实现注入锁定, 形成高阶亚谐波注入锁定光电振荡器。搭建实验系统, 当注入亚谐波射频信号功率 17.5 dBm、频率范围 4.8 GHz~5.2 GHz 时, 光电振荡器的五次亚谐波注入锁定, 实现了 K 波段 24~26 GHz 频率范围内可调谐输出, 各输出信号的边模抑制比均优于 70 dB, 相位噪声 10 Hz 偏频处低于 -70 dBc/Hz, 10 kHz 偏频处低于 -129 dBc/Hz。

**关键词:** 双偏振马赫-曾德尔调制器; 注入锁定; 五阶亚谐波; 可调谐; 光电振荡器

中图分类号: TN29

文献标识码: A

doi: 10.3788/gzxb20265503.0355111

## 0 引言

现代通信、雷达及电子战等领域的快速发展, 对微波信号的频谱纯度、相位噪声、频率调谐范围及高频覆盖能力提出了更高要求<sup>[1-4]</sup>。传统电子振荡器(如石英振荡器)<sup>[5-9]</sup>通常需通过多级倍频产生高频信号, 在此过程中相位噪声会以  $20\log N$  ( $N$  为倍频次数) 的规律恶化, 限制了其在高频系统中的应用。光电振荡器 (Optoelectronic Oscillator, OEO) 利用光电反馈环路产生微波信号, 具有相位噪声低、与振荡频率无关的独特优势, 成为实现高频、高稳微波输出的重要方案。

自 1996 年 YAO X S 和 MALECKI L 首次提出 OEO 概念以来<sup>[10-18]</sup>, 其高频化研究不断推进。K 波段 (通常指 18~27 GHz) 因其较宽的可用带宽、紧凑的天线尺寸, 以及在卫星通信、高分辨率雷达和未来 5G/6G 移动系统中的重要应用潜力, 被视为高频段系统研究的理想选择之一。2010 年, FEDDERWITZ S 等实现了 20.7~21.8 GHz 可调谐 OEO<sup>[19]</sup>; 2012 年, 孙斌等发展了双环路结构以产生 20 GHz 信号<sup>[20]</sup>。这些早期工作为 K 波段 OEO 的发展奠定了基础, 但系统结构复杂且性能有限。近年来, 基于双布里渊移频器<sup>[21]</sup>与薄膜铌酸锂集成平台<sup>[22]</sup>的 OEO 相继提出, 分别在固定频率与可调谐输出方面取得进展, 但仍面临频率覆盖有限或环境稳定性不足的挑战。

然而受限于高品质因数 (Quality Factor, Q) 的射频滤波器, 传统 OEO 在高频段易出现多模振荡与频率跳变, 导致边模抑制比下降与频率失稳。注入锁定技术可有效抑制边模、稳定输出<sup>[23-27]</sup>, 但其要求注入信号与 OEO 自由振荡频率接近, 在高频段往往依赖昂贵且复杂的高频信号源, 这制约了该技术向高频段发展。

为此, 本文提出一种基于双偏振马赫-曾德尔调制器 (Dual-Polarization Mach-Zehnder Modulator, Dpol-

基金项目: 河北省自然科学基金 (F2024201002), 河北大学自然科学多学科交叉研究计划资助项目 (DXK202204)

第一作者: 赵晓鹏, 2623639820@qq.com

通讯作者: 郝鹏, haopeng@hbu.edu.cn

收稿日期: 2025-11-20; 录用日期: 2026-01-08

<http://www.photon.ac.cn>

MZM)的K波段五阶亚谐波注入锁定OEO方案。该系统利用Dpol-MZM两个偏振态的独立性,在X偏振态中通过外注入射频信号产生高次谐波,经滤波产生五次谐波后,再将其注入基于Y偏振态构建的OEO环路,实现亚谐波注入锁定。该方法将谐波倍频与注入锁定有效结合,仅利用低频信号源即可产生高频率、可调谐、高频谱纯度与优异频率稳定性的微波信号,为高频微波光子的实际应用提供了一条可行路径。

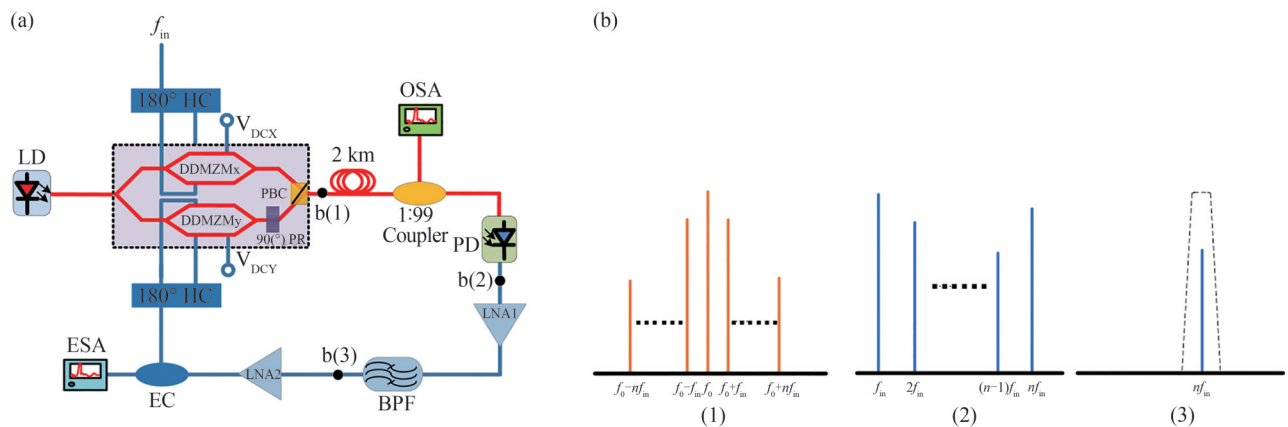
## 1 实验原理

### 1.1 系统结构

本文提出的高阶亚谐波注入锁定光电振荡器系统结构如图1(a)所示,激光器输出的光信号注入Dpol-MZM。Dpol-MZM将输入光分为两路独立传输的光信号,其中一路光保持原偏振方向(X偏振态),另一路则通过Dpol-MZM内部偏振旋转器将偏振方向旋转 $90^\circ$ (Y偏振态),最终通过偏振合束器将两路光信号合并至同一光纤中传输,构成了系统的双偏振并行光路。Dpol-MZM输出的光信号同时包含X和Y两个正交偏振态。该信号通过单模光纤环进行传输,与常被认为更适合偏振保持的保偏光纤相比,单模光纤环在此场景下展现出独特优势。保偏光纤虽能维持偏振态,但其使用中存在显著的对轴问题:即光纤的双折射轴必须与入射光的偏振方向精确对准,任何偏差都会引入额外的偏振串扰和损耗,增加了系统实验过程中的难度。而单模光纤环在保证X、Y偏振态光信号偏振方向相互垂直的前提下,能够以较低的传输损耗实现信号的稳定环路传输。这一特性得益于单模光纤环中偏振态相对稳定可控,并可在环路内维持两路偏振信号的分离性与正交性,从而在避免复杂对轴工艺的同时,满足系统对偏振复用传输的基本要求。

射频信号 $f_m$ 注入DDMZMx对X偏振态光进行调制,如图1(b)(1)所示,调制后的光谱中包含光载波及各阶边带。该光信号经光电探测器(Photodetector, PD)进行光电转换后,产生 $f_m$ 的各次谐波分量,其频谱示意图如图1(b)(2)所示。通过低噪声放大器与中心频率为 $nf_m$ 的带通滤波器后,将 $n$ 次谐波信号筛选并放大,如图1(b)(3)所示,在此过程中低频的注入信号 $f_m$ 转换为了 $n$ 倍频的高频信号。

经滤波放大后频率为 $nf_m$ 的高频信号,注入DDMZMy的射频端口。DDMZMy与光电探测器、带通滤波器、射频放大器及电耦合器等元件共同构成一个完整的OEO环路。当该环路增益满足起振条件且相位匹配时,环路将仅在 $nf_m$ 频率上产生并维持稳定的振荡信号,从而实现亚谐波注入锁定,最终通过电耦合器即可输出一个频率为 $nf_m$ 的高纯度微波信号。因此该系统通过Dpol-MZM光域的偏振复用,将微波信号倍频



LD: Laser Diode; PD: Photodetector; EC: Electronic Coupler; LNA: Low Noise Amplifier; BPF: Bandpass Filter; OSA: Optical Signal Analyzer; ESA: Electrical Signal Analyzer;  $180^\circ$ HC:  $180^\circ$  Hybrid 3 dB Coupler

图1 亚谐波产生原理及系统示意图。(a)亚谐波注入锁定光电振荡器系统原理示意图;(b)高阶亚谐波产生示意图:(1)向Dpol-MZM中X偏振态调制器注入射频信号后X偏振态的光谱示意图;(2)调制后的光信号在PD光电转换后的频谱示意图;(3)经宽带滤波器滤波和射频放大器放大后的高阶亚谐波示意图

Fig.1 Principle of subharmonic generation and system schematic diagram. (a) Schematic diagram of a subharmonic injection-locked optoelectronic oscillator system; (b) Diagram of high harmonic generation: (1) Optical spectrum schematic of the RF-modulated X-polarization state in a Dpol-MZM; (2) Schematic diagram of the spectrum after PD conversion of the modulated optical signal; (3) Schematic of the high-order subharmonic after filtration by a broadband filter and amplification by an RF amplifier

和注入锁定 OEO 的优势结合到了一起,能够在不利用高频信号源的情况下产生高质量、高频率、可调谐、高频率稳定性和边模抑制比良好的射频信号。

## 1.2 理论分析

X 偏振态调制器的光场强度可表示为

$$E_X = \frac{E_0 e^{j\omega_0 t}}{2\sqrt{2}} [e^{i\beta \sin \omega_{RF} t} + e^{i[\beta \sin(\omega_{RF} t + \varphi) + \theta]}] \quad (1)$$

式中,  $\beta$  为调制指数,  $\beta = \pi \frac{V_1}{V_{\pi RF}}$ ,  $V_1$  为输入射频信号的电压,  $V_{\pi RF}$  为 X 偏振态调制器射频的半波电压。  $\theta = \pi \frac{V_2}{V_{\pi DC}}$ ,  $V_2$  为直流偏置电压,  $V_{\pi DC}$  为 X 偏振态调制器直流的半波电压,  $\varphi$  为输入两路射频信号间的相位差,  $\omega_{RF}$  为输入射频信号的角频率。经过 PD 后

$$i_X \propto E_X \times E_X^* = \frac{E_0^2}{8} \{ 2 + 2 \{ [J_0(\delta) + 2 \cos \theta \sum_{n=1}^{\infty} J_{2n}(\delta) \cos [2n(\omega_{RF} t - \Delta)] + 2 \sin \theta \sum_{n=1}^{\infty} J_{2n-1}(\delta) \sin [(2n-1)(\omega_{RF} t - \Delta)] \} \} \quad (2)$$

式中,  $\delta = \sqrt{2\beta^2(1 - \cos \varphi)}$ ,  $\cos \Delta = \frac{\beta - \beta \cos \varphi}{\delta^2}$ 。通过式(2)结果可以看出第  $n$  阶边带的射频功率由  $\theta$  和

$J_n(\delta)$  共同所决定。因此当  $\sin \theta$  绝对值最大时,  $\theta = \frac{\pi}{2} + m\pi$ ,  $m$  为整数, 此时偏置在正交工作点; 当  $\cos \theta$  绝对值最大时,  $\theta = m\pi$ ,  $m$  为整数, 此时偏置在最大工作点。同时  $\delta$  的值越大,  $J_n(\delta)$  越大, 高阶边带的射频功率越高, 因此  $\varphi = \pi + 2m_1\pi$ ,  $m_1$  为整数, 即射频两路信号相位之间应相差  $180^\circ$ 。在此条件下第  $n$  阶边带经 PD 拍频后的功率  $P_n \propto [J_n(2\beta)]^2$ , 因此对应任意两阶边带的功率,  $P_a - P_b = 20 \lg \frac{J_a(2\beta)}{J_b(2\beta)}$ ,  $a, b$  为任意正整数。

当频率为  $P_{inj} = nf_{in}$  的高次谐波信号从 X 偏振态产生并注入基于 Y 偏振态构建的 OEO 环路后, 若该频率与环路的自由振荡频率  $f_0$  足够接近, OEO 的输出频率将被牵引至  $f_{inj}$ , 并为之保持同步。锁频带宽  $\Delta f_L$  可表示为

$$\Delta f_L \approx \frac{f_0}{2Q} \cdot \frac{1}{\sqrt{P_{osc}/P_{inj}}} \quad (3)$$

式中,  $Q$  为振荡器的品质因数,  $P_{osc}$  与  $P_{inj}$  分别为振荡功率与注入功率。通过精确控制注入射频信号的功率与频率, 使  $nf_{in}$  满足

$$|nf_{in} - f_0| < \Delta f_L \quad (4)$$

即可实现亚谐波注入锁定, 锁定后, OEO 将稳定输出频率为  $nf_{in}$  的射频信号。

## 2 实验结果

根据图 2 所示, 本实验使用保偏激光器(NKT Photonics Basik E15), 其中心波长在 1 550 nm 附近, 输出功率为 16.02 dBm, 输出的保偏激光进入 Dpol-MZM 后分为 X、Y 两个偏振态的相同两束。Dpol-MZM (Fujitsu FTM7980EDA) 具有 20 GHz 的 3 dB 带宽并在每个偏振态上有至少 20 dB 的消光比。X 偏振态的射频输入端口由射频信号源 (Keysight N5183B, 输出频率范围 9 kHz~20 GHz, 最高输出功率到 25 dBm) 输入射频信号。根据上述理论分析 X 偏振态调制器直流端口应根据倍频数的奇偶设置在正交工作点或最大工作点, 同时两路射频信号间相差  $180^\circ$  的相位差, Y 偏振态调制器设置在正交工作点使光电振荡器工作在线性区。实验中采用光谱分析仪(APEX AP2051A)通过一个 1:99 光耦合器对系统的光谱进行测量。光电探测器的工作范围为 0~40 GHz, 用于将加载射频的光信号转化为电信号。宽带滤波器(康迈微 ZBF4-C25-2G-750)通带范围为 24~26 GHz, 其阻带抑制度大于 55 dB, 由于光学滤波器的带外抑制比和插损等性能指标难以满足系统要求, 因此该滤波器对系统高次谐波的滤出和 OEO 的模式选择具有重要作用。第一级低噪声放大器(泰莱微波 TLLA18G40G-36-30)工作频率范围为 18~40 GHz, 增益为 36 dB; 第二级低噪声放大器

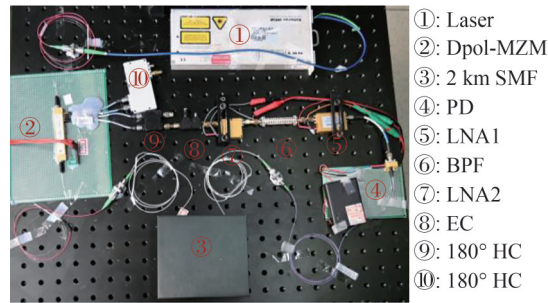


图2 亚谐波注入锁定光电振荡器系统实验装置实物图

Fig.2 Photograph of the experimental setup for a subharmonic injection-locked optoelectronic oscillator

(泰莱微波 TLPA10M40G-20-20)工作频率范围为 10 MHz~40 GHz,增益为 28 dB,其噪声指数和加性噪声将直接影响 OEO 信号的相位噪声。实验中采用相位噪声分析仪(Rohde&Schwarz:FSWP26)通过一个 1:9 电耦合器对系统输出的微波信号进行频率和相位噪声的测量。

为验证注入锁定过程,首先在 Dpol-MZM 输出端接入一个保偏偏振分束器,分别观测 X 与 Y 偏振态的独立光谱。当向 DDMZMx 注入频率为 5 GHz、功率为 17.5 dBm 的射频信号,并将其偏置在正交工作点时,测得 X 偏振态的输出光谱如图 3(a)所示。由于调制器内部存在有限的偏振串扰,在 Y 偏振态光谱中同样观测到来自注入信号的调制边带,其光谱如图 3(b)所示。这些边带的功率显著低于 X 偏振态,表明串扰水平

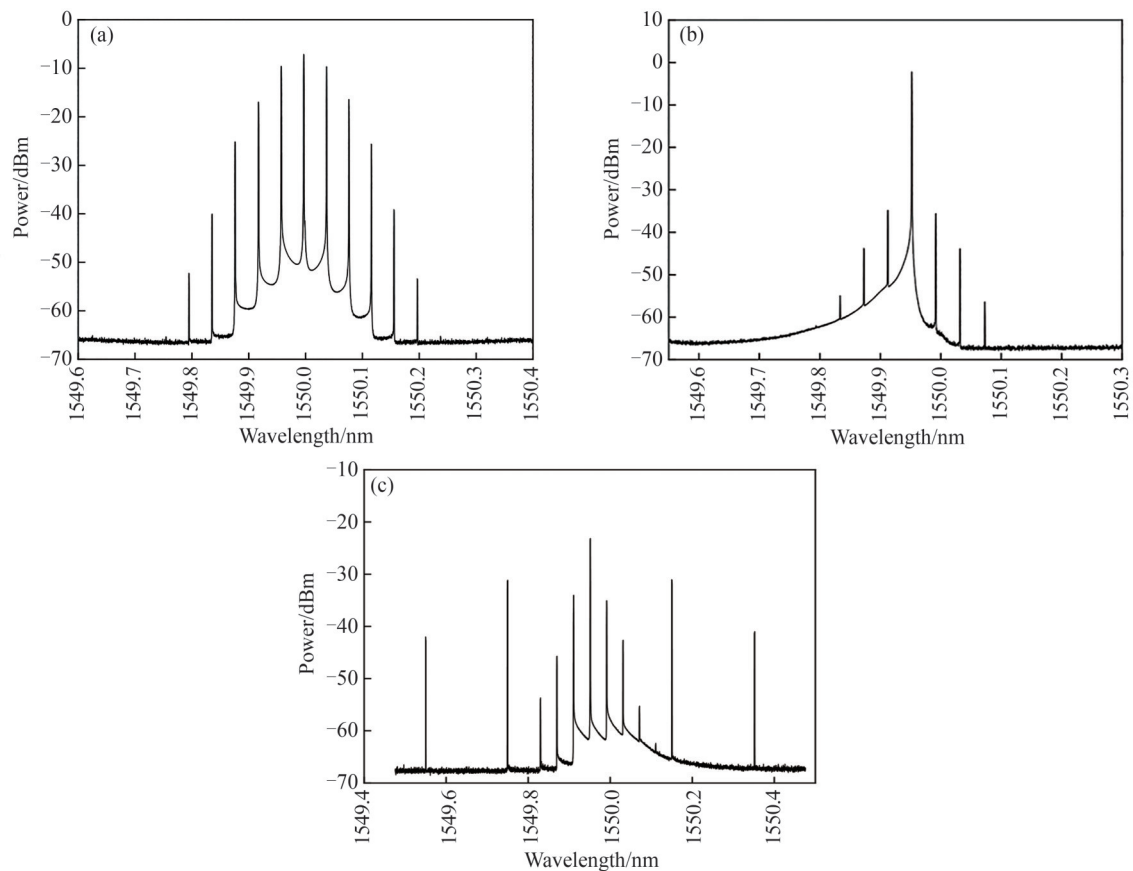


图3 亚谐波注入锁定光电振荡器光谱分析。(a)向X偏振态调制器注入17.5 dBm射频信号后经PBS分束得到的X偏振态光谱;(b)向X偏振态调制器注入17.5 dBm射频信号后经PBS分束得到的Y偏振态光谱;(c)五阶亚谐波注入锁定后通过1:99耦合器测量得到的OEO光谱

Fig.3 Spectral analysis of a subharmonic injection-locked optoelectronic oscillator (a) X-polarization optical spectrum via PBS splitting with 17.5 dBm RF signal injection into X-polarization modulator; (b) Y-polarization optical spectrum via PBS splitting with 17.5 dBm RF signal injection into X-polarization modulator; (c) OEO spectrum measured via a 1:99 coupler under fifth-order subharmonic injection locking

得到有效控制。随后,移除PBS,将实验系统恢复至图1(a)所示的完整OEO链路。当环路达到稳定振荡状态时,通过1:99光耦合器测得的总输出光谱如图3(c)所示。与图3(a)对比可见,五阶边带(对应25 GHz)的功率得到显著增强,而其他边带功率相对下降,这表明五阶谐波信号已成功注入并锁定OEO环路。

为验证系统谐波的产生与滤波,在偏振分束器后接入PD,对X偏振态支路输出信号进行频谱测量。当向DDMZMx注入频率为5 GHz、功率为17.5 dBm的射频信号,且调制器偏置于正交工作点时,测得PD输出频谱如图4(a)所示。在此偏置条件下有效抑制了偶次谐波分量,同时使奇次谐波功率最大化。由于实验中射频注入功率17.5 dBm,  $V_{\pi\text{RF}}$  约为4.25 V,根据公式  $\beta = \frac{V}{V_{\pi}}$  计算可得  $\beta = 1.24$ ,因此  $P_3 - P_5 = 20.65$  dB,同理可得  $P_1 - P_3 = 5.74$  dB。根据图4(a)可知,一阶、三阶、五阶亚谐波的功率分别为-21.98 dBm、-27.12 dBm、-48.43 dBm,计算可得  $P_1 - P_3 = 5.14$  dB,  $P_3 - P_5 = 21.31$  dB,综上在误差范围内理论计算与实验结果相吻合。

将该信号接入中心频率为25 GHz、带宽为2 GHz的带通滤波器进行滤波,滤波后频谱如图4(b)所示。测量结果表明,滤波器有效滤除了基频和其他谐波分量,仅保留五倍频信号并通过后续放大器将其功率显著提升。经滤波放大后,25 GHz信号功率较滤波前提升超过45 dB,而其余频率分量被抑制至噪声基底以下,带外抑制比优于55 dB。这一结果验证了系统能够有效从多次的谐波频谱中滤出目标高频分量,为后续注入锁定过程提供了纯净且具备足够功率的注入信号。该过程成功将5 GHz的低频外注入信号转换为25 GHz的高频信号,展现了系统通过谐波生成方式实现倍频的有效性,为后续OEO环路的注入锁定奠定了基础。

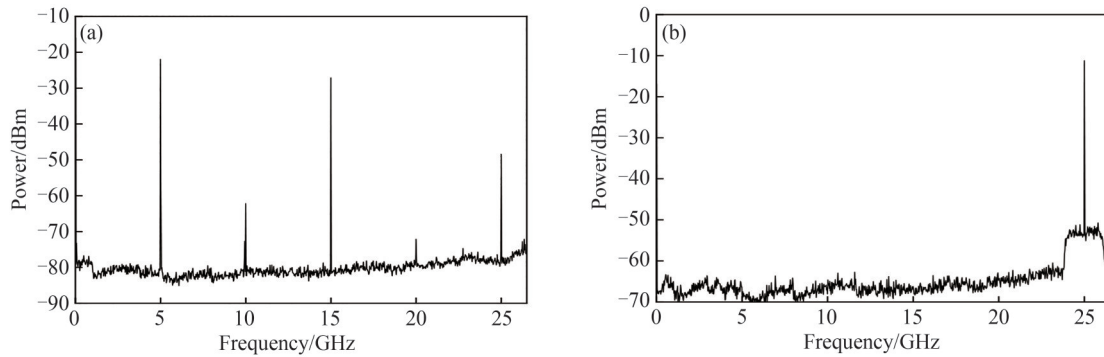


图4 亚谐波注入锁定光电振荡器频谱分析。(a)向X偏振态调制器注入17.5 dBm射频信号后经光电探测器拍频所获得的频谱;(b)该信号经射频放大器放大与宽带滤波器滤波后得到的频谱。

Fig.4 Spectral analysis of a subharmonic injection-locked optoelectronic oscillator. (a) Spectrum obtained from optical beat note detection via a photodetector following 17.5 dBm RF signal injection into the X-polarization modulator; (b) Spectrum after amplification by an RF amplifier and filtering by a bandpass filter

为验证系统注入锁定状态下输出信号的性能参数,通过180°电桥耦合器向X偏振态调制器注入射频信号,在固定注入功率为17.5 dBm的条件下,通过精确调节注入信号的频率,成功在宽带滤波器通带范围内的五个频率处实现了稳定的注入锁定。实验结果显示,当注入信号频率分别设置为4.8 GHz、4.9 GHz、5.0 GHz、5.1 GHz和5.2 GHz时,系统相应地在24.0 GHz、24.5 GHz、25.0 GHz、25.5 GHz和26.0 GHz处产生稳定的单模振荡输出。各锁定状态下的输出频谱如图5所示,测量范围覆盖了注入中心频率附近1 GHz的频带。并且所有五个频率处的主模功率均大于0 dBm,且功率波动被控制在1 dB范围内。需要特别说明的是,受限于实验中采用的射频信号源输出功率及系统内各器件的频率响应特性,当前系统最高实现了五倍频的谐波注入锁定。当DDMZMx偏置在正交工作点时,五次谐波分量达到最大,这与第1.2节中的理论分析完全一致。该实验结果验证了基于Dpol-MZM的亚谐波注入锁定方案在产生高频微波信号方面的可行性和有效性。

为全面评估系统在调谐范围内的频谱纯度与稳定性,对24.0 GHz、24.5 GHz、25.0 GHz、25.5 GHz和26.0 GHz五个频率处的输出频谱进行了精细测量,结果如图6(a)~(e)所示。所有测量均在注入锁定状态下完成,射频注入信号频率分别设置为4.8 GHz、4.9 GHz、5.0 GHz、5.1 GHz和5.2 GHz,注入功率稳定在17.5 dBm左右。实验结果显示,在该范围内系统均能实现稳定的单模振荡。各频点输出信号的边模抑制比均优于

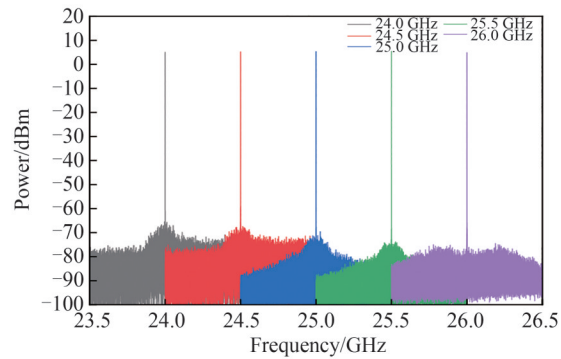
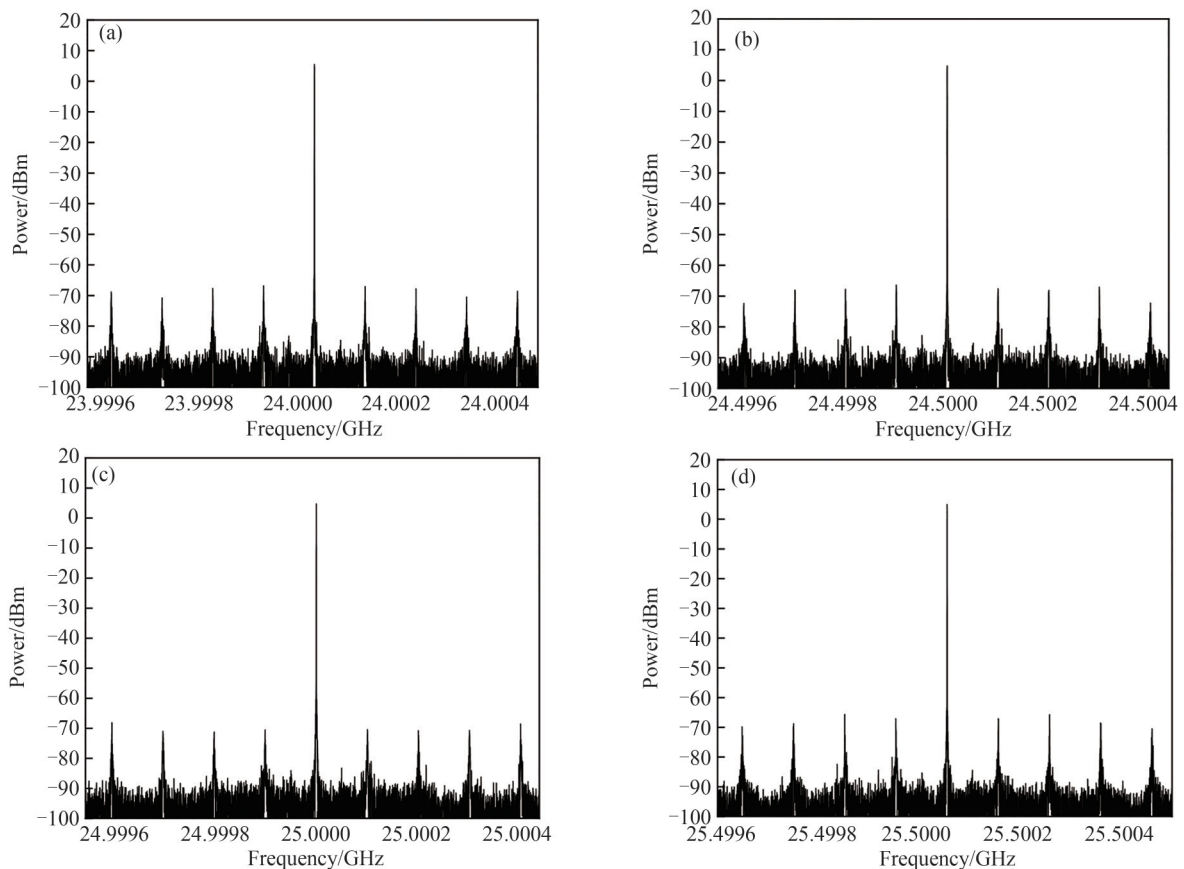


图5 五阶亚谐波注入锁定后OEO在24.0 GHz、24.5 GHz、25.0 GHz、25.5 GHz和26.0 GHz五个频率处的输出频谱图  
Fig.5 Output spectrum of the OEO at 24.0 GHz, 24.5 GHz, 25.0 GHz, 25.5 GHz and 26.0 GHz under fifth-order subharmonic locking

70 dB,这一优异的边模抑制性能验证了注入锁定机制的有效性,在外界信号注入后,系统能量被有效地集中于主模,同时显著抑制了由长光纤环路引起的多模振荡问题。进一步观察发现,五个频率的输出功率波动范围小于1 dB,表明系统在宽频带调谐过程中保持了良好的增益平坦度。各频谱波形纯净,且在分辨率带宽为100 Hz的设置下,频谱基底均保持在-90 dBm以下,这反映了系统具有极低的固有噪声水平。与未采用注入锁定的传统OEO系统相比,本方案边模抑制比有了明显的提升,这一显著改善直接证实了亚谐波注入锁定策略在提升高频OEO频谱纯度方面的优势。高边模抑制比结合良好的功率一致性表明,基于Dpol-MZM的偏振复用成功实现了谐波注入与振荡环路的稳定产生,确保了系统在K波段宽范围内调谐时仍能保持卓越的频谱性能。

相位噪声是评估微波信号的关键指标,为全面表征注入锁定后OEO的输出性能,对上述五个频率处的相位噪声进行了测量,结果如图7(a)所示。在10 Hz至1 MHz的频偏范围内,各频率的相位噪声曲线呈现高度一致性,表明OEO在锁定状态下的相位噪声特性与振荡频率无关,这证明了亚谐波注入锁定方案的可行



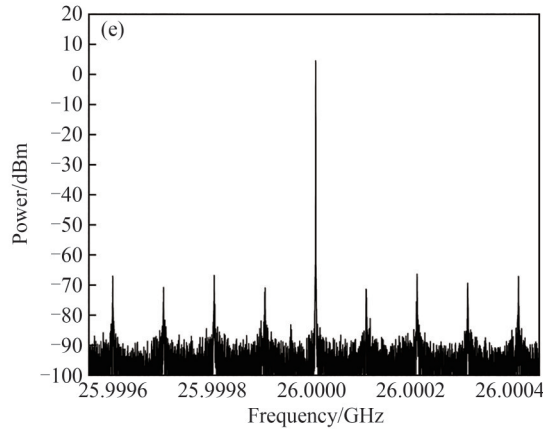


图6 五阶亚谐波注入锁定后OEO在(a) 24 GHz, (b) 24.5 GHz, (c) 25 GHz, (d) 25.5 GHz, (e) 26 GHz的输出频谱  
Fig.6 Fifth-order subharmonic injection-locked OEO output spectrum measured at (a) 24 GHz, (b) 24.5 GHz, (c) 25 GHz, (d) 25.5 GHz, (e) 26 GHz

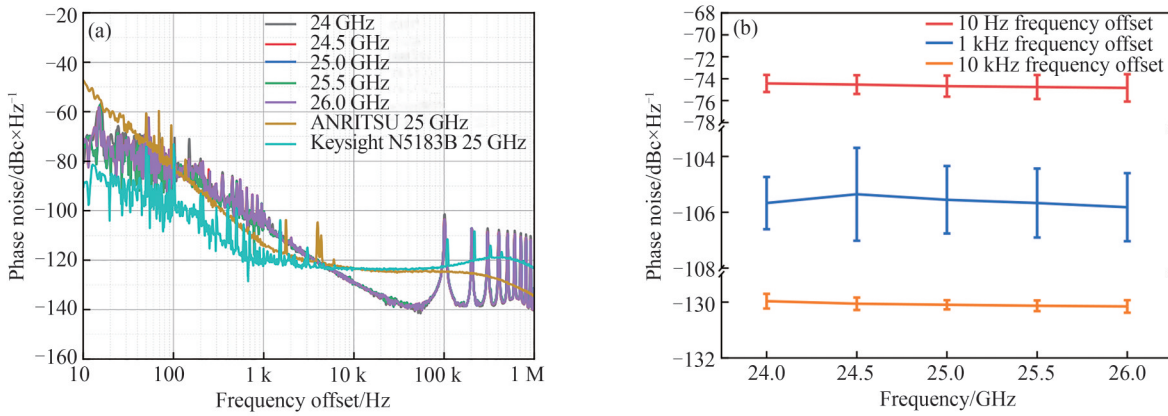


图7 五阶亚谐波注入锁定光电振荡器输出信号相位噪声特性。(a) 五阶亚谐波注入锁定后OEO相位噪声测试曲线；  
(b) 五阶亚谐波注入锁定后相位噪声误差情况  
Fig.7 Phase noise characteristics of the output signal from a fifth-order subharmonic injection-locked optoelectronic oscillator.  
(a) Phase noise measurement of the OEO under fifth-order subharmonic injection locking; (b) Fifth-order subharmonic injection-locked phase noise performance

性。作为对比,测量了商用高频信号源 ANRITSU MG36241A 在 25 GHz 输出时的相位噪声特性。其在 10 Hz 和 10 kHz 偏移处的相位噪声略高于本系统输出信号,而在 1 kHz 偏移处表现更优。同时,对本实验使用的 Keysight N5183B 信号源 5 GHz 输出的相位噪声进行了测量,结果显示在 10 Hz 偏移处接近  $-90$  dBc/Hz, 10 kHz 偏移处与 ANRITSU MG36241A 的 25 GHz 输出相当。理论上,五倍频过程将使相位噪声恶化约 14 dB,且实际系统中射频和光学器件的噪声会进一步恶化信号质量。因此,经过五倍频后的注入信号相位噪声将显著低于市售高频信号源,若采用 ANRITSU 信号源直接提供高频注入信号,预计可进一步提升锁定后 OEO 的输出性能。

对锁定状态下输出信号的相位噪声进行了重复性验证,结果如图 7(b) 所示。在 10 Hz、1 kHz 和 10 kHz 三个频偏处绘制的误差棒显示:10 Hz 处的相位噪声稳定在  $-75$  dBc/Hz 附近,表明输出信号的近端相位噪声被锁定在注入信号源上;10 kHz 处的相位噪声稳定在  $-130$  dBc/Hz,说明输出信号的远端相位噪声未受倍频过程影响,保持了 OEO 自由运行时的低噪声特性。1 kHz 处的相位噪声则稳定在  $-105$  dBc/Hz 左右,由于本实验过程中使用的射频信号源存在噪声,这部分噪声会通过电光调制过程转移至光边带,并最终经光电探测与高次谐波进入 OEO 环路,导致系统在 1 kHz 偏移处的相位噪声出现波动,从而相较于频偏 10 Hz 和 10 kHz 处,该频偏处相位噪声多次测量的误差结果较大。

为评估注入锁定后 OEO 输出信号的频率稳定性,采用艾伦方差(Allan Deviation)作为关键指标,对五个

锁定频率处(24.0 GHz、24.5 GHz、25.0 GHz、25.5 GHz、26.0 GHz)的输出信号进行了系统测量。该指标能够有效反映振荡器在不同时间尺度下的频率稳定性,尤其适用于评估光电振荡系统的短期至中期稳定性。测量结果如图8所示,横轴为平均时间 $\tau$ ,覆盖 $1\ \mu\text{s}$ 至 $10\ \text{s}$ 的范围,纵轴为对应平均时间下的艾伦方差值。图中显示,五个频率处所对应的艾伦方差曲线高度重合,在整体趋势上表现出极好的一致性。该现象说明,系统在 $24\ \text{GHz}\sim 26\ \text{GHz}$ 范围内均具备频率稳定性能,不随输出频率的改变而发生显著波动。其艾伦方差在 $1\ \mu\text{s}$ 到接近 $1\ \text{s}$ 的范围内随参考信号源整体下移,当 $\tau$ 接近 $1\ \text{s}$ 时,曲线结束下降趋势,并开始逐步上翘,这是由于在短时间内注入锁定光电振荡器输出信号的频率稳定性主要受参考信号源支配。由于注入锁定作用,其艾伦方差曲线整体随参考信号源的艾伦方差曲线下移,并逐渐趋近于参考信号源的艾伦方差曲线,此时系统表现出良好的短期稳频特性。然而随着平均时间 $\tau$ 的进一步延长,参考信号源的影响逐渐减弱,而光纤链路自身固有的长时不稳定因素开始主导系统性能。其中,温度波动、机械应力松弛等因素引起的光纤漂移所引入的相位噪声逐渐累积,导致输出信号的频率漂移加剧。这一效应反映在艾伦方差曲线上,即表现为曲线逐渐偏离参考信号源的下降趋势,转而呈现明显的上翘特征。

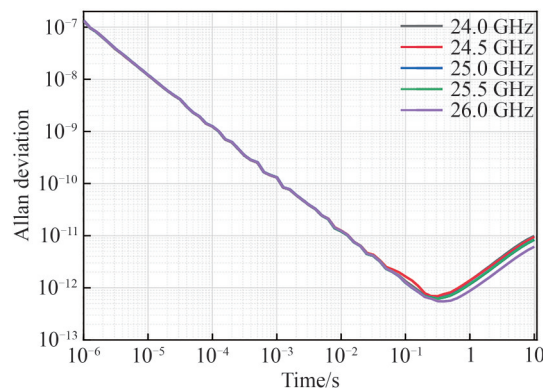


图8 五阶亚谐波注入锁定后OEO输出信号在24 GHz、24.5 GHz、25 GHz、25.5 GHz、26 GHz五个频率处 $1\ \mu\text{s}\sim 10\ \text{s}$ 内的艾伦方差测试曲线

Fig.8 Allan deviation of the OEO output signal measured at 24 GHz, 24.5 GHz, 25 GHz, 25.5 GHz, 26 GHz for time intervals from  $1\ \mu\text{s}$  to  $10\ \text{s}$ , under fifth-order subharmonic injection locking.

### 3 结论

本文提出并实验验证了一种基于双偏振马赫-曾德尔调制器的五阶亚谐波注入锁定光电振荡器。该系统通过将低频射频信号注入X偏振态以产生五次谐波,并将其作为锁定信号反馈至基于Y偏振态构建的OEO环路,成功实现了在无需高频信号源条件下产生K波段( $24\ \text{GHz}\sim 26\ \text{GHz}$ )可调谐微波信号。实验结果表明,锁定后的输出信号边模抑制比高于 $70\ \text{dB}$ ,在 $10\ \text{Hz}$ 和 $10\ \text{kHz}$ 频偏处的相位噪声分别低于 $-70\ \text{dBc}/\text{Hz}$ 与 $-129\ \text{dBc}/\text{Hz}$ 。与传统的倍频方案相比,本系统在实现五倍频程的同时,有效避免了相位噪声随倍频次数恶化的固有缺陷,其近端相噪由注入信号决定,远端相噪则维持了OEO固有的低噪声水平。该方案在原理上对输出频率没有上限限制。然而,受实验中所用器件的带宽、功率与频率响应限制,当前系统的调谐范围被约束在 $24\ \text{GHz}\sim 26\ \text{GHz}$ 。若未来采用更高带宽与功率限制的光学与射频器件,或引入多级调制器级联结构,有望实现更高阶次谐波的生成与锁定,从而将输出频率拓展至太赫兹波段。尽管后者将带来更复杂的系统设计与参数优化挑战,但无疑为高性能高频信号源提供了一条极具潜力的技术路径。

#### 参考文献

- [1] PENG Z, LI C. Portable microwave radar systems for short-range localization and life tracking: a review[J]. Sensors, 2019, 19(5): 1136.
- [2] PAN S, ZHANG Y. Microwave photonic radars[J]. Journal of Lightwave Technology, 2020, 38(19): 5450-5484.
- [3] BRANDÃO T H, SCOTTI F, FILGUEIRAS H R D, et al. Coherent dual-band radar system based on a unique antenna and a photonics-based transceiver[J]. IET Radar, Sonar & Navigation, 2019, 13(4): 505-511.
- [4] SCOTTI F, LAGHEZZA F, GHELFI P, et al. Multi-band software-defined coherent radar based on a single photonic transceiver[J]. IEEE Transactions on Microwave Theory and Techniques, 2015, 63(2): 546-552.

- [5] NICODIMUS R A, TAKAGI S, FUJII N. Wide tuning range voltage-controlled ring oscillator[J]. *IEICE Transactions on Electronics*, 2003, 86(6): 1085-1088.
- [6] KOMINE V, GALLIOU S, MAKAROV A. A parametric quartz crystal oscillator[J]. *IEEE Transactions on Ultrasonics, Ferroelectrics, and Frequency Control*, 2003, 50(12): 1656-1661.
- [7] SALZENSTEIN P, KUNA A, SOJDR L, et al. Significant step in ultra-high stability quartz crystal oscillators [J]. *Electronics Letters*, 2010, 46(21): 1433-1434.
- [8] LOCKE C R, IVANOV E N, HARTNETT J G, et al. Invited article: design techniques and noise properties of ultrastable cryogenically cooled sapphire-dielectric resonator oscillators[J]. *Review of Scientific Instruments*, 2008, 79(5): 051301.
- [9] HARTNETT J G, NAND N R, LU C. Ultra-low-phase-noise cryocooled microwave dielectric-sapphire-resonator oscillators[J]. *Applied Physics Letters*, 2012, 100(18): 183501.
- [10] FAN Feng, JIANG Yang, YU Jinlong, et al. Tunable optoelectronic oscillator based on stimulated Brillouin scattering and a coupled dual-loop structure[J]. *Acta Photonica Sinica*, 2019, 48(8): 0823001.  
范峰, 江阳, 于晋龙, 等. 基于受激布里渊散射和耦合型双环的可调谐光电振荡器[J]. *光子学报*, 2019, 48(8): 0823001.
- [11] TONG Guochuan, WANG Zhengli, YANG Zhen, et al. Research on stability of broadband tuning optoelectronic oscillator based on intermediate frequency phase locking technology[J]. *Acta Photonica Sinica*, 2018, 47(11): 1123001.  
童国川, 王正丽, 杨振, 等. 基于中频相位锁定技术的宽带调谐光电振荡器稳定性研究[J]. *光子学报*, 2018, 47(11): 1123001.
- [12] LAI Tianhao, JIANG Yang, YU Jinlong, et al. Improving the stability of an optoelectronic oscillator based on self-phase locking technology[J]. *Acta Photonica Sinica*, 2018, 47(1): 0123001.  
来天皓, 江阳, 于晋龙, 等. 基于自相位锁定技术提升光电振荡器的稳定性[J]. *光子学报*, 2018, 47(1): 0123001.
- [13] BAI Guangfu, JIANG Yang, HU Lin. Tunable optoelectronic oscillator based on injection-locking effect in DFB cavity [J]. *Acta Photonica Sinica*, 2017, 46(5): 0523004.  
白光富, 江阳, 胡林. 基于DFB腔注入锁定效应的可调谐光电振荡器[J]. *光子学报*, 2017, 46(5): 0523004.
- [14] ZHENG Junchao, YANG Chun, QIAO Guanyu, et al. Comparison and optimization of phase-locked loop and injection-locking techniques in optoelectronic oscillators[J]. *Acta Photonica Sinica*, 2017, 46(4): 0423002.  
郑俊超, 杨春, 乔冠宇, 等. 光电振荡器中锁相环和注入锁定技术的比较和优化[J]. *光子学报*, 2017, 46(4): 0423002.
- [15] CHEN Meng, YANG Chun, ZHENG Junchao, et al. Tunable optoelectronic oscillator based on planar lightwave circuit resonator[J]. *Acta Photonica Sinica*, 2017, 46(4): 0423001.  
陈猛, 杨春, 郑俊超, 等. 基于平面光波导谐振腔的可调谐光电振荡器[J]. *光子学报*, 2017, 46(4): 0423001.
- [16] CAO Zhewei, YANG Chun, ZHOU Zhenghua. High performance injection-locked phase optoelectronic oscillator [J]. *Acta Photonica Sinica*, 2017, 46(1): 0123002.  
曹哲玮, 杨春, 周正华. 高性能注入锁相光电振荡器[J]. *光子学报*, 2017, 46(1): 0123002.
- [17] REN Fengxin, JIANG Yang, YU Jinlong, et al. Method for improving long-term stability of optoelectronic oscillator based on feedback control loop[J]. *Acta Photonica Sinica*, 2015, 44(10): 1023003.  
任凤鑫, 江阳, 于晋龙, 等. 基于反馈控制环路提高光电振荡器长期稳定性的方法[J]. *光子学报*, 2015, 44(10): 1023003.
- [18] YAO X S, MALECKI L. Converting light into spectrally pure microwave oscillation[J]. *Optics Letters*, 1996, 21(7): 483-485.
- [19] FEDDERWITZ S, STÖHR A, BABIEL S, et al. Optoelectronic K-band oscillator with gigahertz tuning range and low phase noise[J]. *IEEE Photonics Technology Letters*, 2010, 22(20): 1497-1499.
- [20] SUN Bin, YU Jinlong, WANG Ju, et al. Highly stable K-band optoelectronic oscillator[J]. *Chinese Journal of Lasers*, 2012, 39(3): 0305010.  
孙斌, 于晋龙, 王菊, 等. K波段高稳光电振荡器[J]. *中国激光*, 2012, 39(3): 0305010.
- [21] LIU P, LIU S, YANG H, et al. K-band optoelectronic oscillator based on a double-Brillouin-frequency shifter [J]. *Optical Engineering*, 2019, 58(10): 100501.
- [22] MA R, HUANG Z, GAO S, et al. Ka-band thin film lithium niobate photonic integrated optoelectronic oscillator [J]. *Photonics Research*, 2024, 12(6): 1283-1293.
- [23] SHUMAKHER E, SHEINMAN B, EISENSTEIN G, et al. Noise properties of harmonically injection locked electronic and optoelectronic oscillators[C]. *Proceedings of the International Topical Meeting on Microwave Photonics*. Budapest, Hungary: IEEE, 2003: 201-204.
- [24] LEE K H, KIM J Y, CHOI W Y. Injection-locked hybrid optoelectronic oscillators for single-mode oscillation [J]. *IEEE Photonics Technology Letters*, 2008, 20(19): 1645-1647.
- [25] BANERJEE A, DE BRITTO L A D, PACHECO G M. Analysis of injection locking and pulling in single-loop

- optoelectronic oscillator[J]. IEEE Transactions on Microwave Theory and Techniques, 2019, 67(5): 2087-2094.
- [26] FAN Z, SU J, LIN Y, et al. Injection locking and pulling phenomena in an optoelectronic oscillator[J]. Optics Express, 2021, 29(3): 4681-4699.
- [27] HASAN M, BANERJEE A, HALL T J. Injection locking of optoelectronic oscillators with large delay[J]. Journal of Lightwave Technology, 2022, 40(9): 2754-2762.

## Tunable High-order Subharmonic Injection-locked Optoelectronic Oscillator in K-band Based on a Dual-polarization Mach-Zehnder Modulator

ZHAO Xiaopeng<sup>1,2</sup>, HUANG Chongjia<sup>1,2</sup>, HAO Peng<sup>1,2</sup>

(1 Photonics Information Innovation Center, College of Physics and Technology, Hebei University, Baoding 071002, China)

(2 Hebei Provincial Center for Optical Sensing Innovations, Baoding 071002, China)

**Abstract:** The advancement of modern communication, radar, and electronic warfare systems imposes stringent requirements on microwave signal sources, including exceptional spectral purity, low phase noise, broad frequency tunability, and operation at high-frequency bands. Conventional electronic oscillators, such as quartz crystal oscillators, typically require multiple frequency-multiplication stages to generate high-frequency signals. This process inherently degrades phase noise by  $20\log N$  (where  $N$  is the multiplication factor), thereby limiting their applicability in high-frequency systems. In contrast, the optoelectronic oscillator employs an optoelectronic feedback loop to generate microwave signals, offering the distinctive advantage of low phase noise that is independent of oscillation frequency. This makes the optoelectronic oscillator a pivotal solution for high-frequency, high-stability microwave generation. Since its inception by YAO X S in 1996, research on high-frequency optoelectronic oscillators has advanced considerably. The K-band (18~27 GHz), with its broad available bandwidth, compact antenna size, and promising applications in satellite communications, high-resolution radar, and future fifth-generation and sixth-generation mobile systems, is regarded as an ideal frequency range for such investigations.

However, conventional optoelectronic oscillators operating at high frequencies are susceptible to multi-mode oscillation and frequency hopping due to the limited quality factor of available radio frequency filters, resulting in degraded side-mode suppression ratio and frequency instability. Injection locking is a well-established technique to suppress side modes and stabilize the output. Nevertheless, it requires an injection signal with a frequency close to the free-running oscillation frequency of the optoelectronic oscillator. At high frequencies, this typically depends on expensive and complex high-frequency signal sources, which hinders the adoption of injection locking in high-frequency optoelectronic oscillators.

This paper proposes and experimentally demonstrates a novel scheme for a fifth-order subharmonic injection-locked optoelectronic oscillator in the K-band, utilizing a dual-polarization Mach-Zehnder modulator. The system exploits the polarization independence of the two optical paths within the dual-polarization Mach-Zehnder modulator. An external, relatively low-frequency radio frequency signal is injected into the modulator that drives the X-polarization state, generating high-order optical sidebands. Following photodetection, the electrical spectrum contains harmonics of the injected signal. A subsequent bandpass filter then selects the fifth harmonic component. This filtered high-frequency signal, precisely at the target K-band frequency (five times the injection frequency), is injected into a conventional optoelectronic oscillator loop constructed using the Y-polarization state of the same dual-polarization Mach-Zehnder modulator. This architecture effectively integrates harmonic frequency multiplication with injection locking within a single, compact photonic configuration. Crucially, it eliminates the need for a dedicated high-frequency signal source for injection, as the high-frequency locking signal is internally generated from a low-frequency input.

An experimental system was implemented to validate the proposed concept. A 1 550 nm laser diode served as the optical source. The dual-polarization Mach-Zehnder modulator provided independent

modulation paths for the  $X$ - and  $Y$ -polarization states. A low-frequency radio frequency signal from a signal generator was injected into the  $X$ -polarization modulator. A photodetector converted the modulated optical signal into an electrical signal. A broadband bandpass filter (24~26 GHz) selected the fifth harmonic, which was then amplified and fed into the optoelectronic oscillator loop formed by the  $Y$ -polarization path; this loop included an additional modulator bias point, a fiber delay line, an amplifier, and a filter. When an injection signal with a power of 17.5 dBm and a tunable frequency range of 4.8~5.2 GHz was applied, the system successfully achieved fifth-order subharmonic injection locking, producing stable single-mode oscillation outputs at 24.0 GHz, 24.5 GHz, 25.0 GHz, 25.5 GHz, and 26.0 GHz, respectively.

The performance of the injection-locked optoelectronic oscillator was thoroughly characterized. Output spectra at all five frequencies exhibited excellent spectral purity, with side-mode suppression ratio values consistently exceeding 70 dB—a significant improvement over free-running optoelectronic oscillators, which are prone to multi-mode oscillation. The output power variation across the 24–26 GHz tuning range was less than 1 dB, indicating good gain flatness. Phase noise measurements revealed outstanding performance: below  $-70$  dBc/Hz at 10 Hz offset and below  $-129$  dBc/Hz at 10 kHz offset for all output frequencies. The near-in phase noise is primarily determined by the quality of the low-frequency injection source, whereas the far-out phase noise retains the inherently low noise floor of the optoelectronic oscillator's long delay line, thereby effectively circumventing the  $20\log N$  degradation associated with pure electronic frequency multiplication. Frequency stability, assessed via Allan deviation measurements over averaging times ( $\tau$ ) from 1  $\mu$ s to 10 s, demonstrated consistent behavior across the five output frequencies. For short averaging times ( $\tau < 1$  s), the stability followed that of the injection source due to the locking effect. For longer  $\tau$ , stability was influenced by environmental perturbations on the fiber delay.

In conclusion, this work successfully demonstrates a tunable, high-performance K-band optoelectronic oscillator based on a dual-polarization Mach-Zehnder modulator-enabled subharmonic injection-locking scheme. The system efficiently generates high-frequency (24~26 GHz), high-spectral-purity microwave signals using only a low-frequency radio frequency source, thereby overcoming key limitations of traditional approaches. The demonstrated performance in terms of side-mode suppression ratio ( $>70$  dB) and phase noise ( $<-70$  dBc/Hz at 10 Hz offset,  $<-129$  dBc/Hz at 10 kHz offset) meets the requirements for advanced microwave systems. Although the current tuning range is constrained by the components employed (filter bandwidth, modulator response), the underlying principle is not inherently frequency limited. Utilizing devices with higher bandwidths or adopting cascaded modulation structures could potentially extend operation to even higher frequencies, including millimeter-wave and terahertz bands. This approach offers a promising and practical photonic pathway toward realizing compact, low-noise, and tunable high-frequency oscillators.

**Key words:** Dual-polarization Mach-Zehnder modulator; Injection locking; Fifth-order sub-harmonic; Tunable; Optoelectronic oscillator

**OCIS Codes:** 250.4110; 230.4910; 060.5625; 250.4110

**CSTR:** 32255.14.gzxb20265503.0355111